Evolution of x-ray resonance Raman scattering into x-ray fluorescence from the excitation of xenon near the L_3 edge

M. A. MacDonald,[1,2,*] S. H. Southworth,[1] J. C. Levin,[1,†] A. Henins,[1] R. D. Deslattes,[1] T. LeBrun,[3] Y. Azuma,[3,‡] P. L. Cowan,[3,§] and B. A. Karlin[4]

[1]*National Institute of Standards and Technology, Gaithersburg, Maryland 20899*

[2]*Engineering and Physical Sciences Research Council, Daresbury Laboratory, Warrington WA4 4AD, United Kingdom*

[3]*Argonne National Laboratory, Argonne, Illinois 60439*

[4]*National Synchrotron Light Source, Brookhaven National Laboratory, Upton, New York 11973*

(Received 2 December 1994)

Near an absorption edge, x-ray emission cannot be treated separately from the absorption process itself; a scattering formalism must be used. Experimental data have been recorded showing x-ray emission from xenon following excitation by tunable synchrotron radiation below and above the L_3 absorption edge. Complete data sets are presented for Xe $L\alpha_{1,2}$ and $L\beta_{2,15}$ emission from 10 eV below to 40 eV above the L_3 edge. In accord with the resonant-inelastic-scattering model, the observed x-ray emission evolves from resonant Raman scattering into characteristic fluorescence as the excitation energy is scanned from below to above the absorption edge.

PACS number(s): 32.30.Rj, 32.70.Jz

INTRODUCTION

At energies far above threshold, photoionization of an atomic inner-shell electron leads to an x-ray-fluorescence spectrum having characteristic energies, intensities, and line shapes. A two-step model, in which the radiative decay process is independent of the photoionization process, is adequate to describe the characteristic fluorescence spectrum. However, as the energy of the incident x ray is lowered to regions near the ionization threshold, the energies, intensities, and line shapes of the emitted x-ray spectrum are modified and are sensitive to the precise energy and bandwidth of the incident x-ray beam. In this case, the "x ray in–x ray out" process may be described as resonant inelastic scattering and the spectrum observed near threshold corresponds to continuous resonance Raman scattering. This has been observed experimentally [1–4], and described theoretically [2,4,5–9]. When the atomic inner-shell vacancy decays through the emission of an Auger electron, the phenomenon is termed the Auger resonant Raman effect and again has been experimentally observed [10–15] and described theoretically [5,9,16].

Excitation to Rydberg orbitals just below an inner-shell ionization threshold may change the position of the Auger or x-ray-fluorescence lines slightly. In this case, the excitation is always resonant, and the exact positions and line shapes of fluorescence or Auger peaks are again dependent on the precise energy and bandwidth of the excitation source. However, with the photoexcited electron still bound in a Rydberg orbital, there is one less degree of freedom available to the system, and the scattering process is analogous to resonance fluorescence, or more properly to the inelastic analogue of resonance fluorescence, and is termed resonance Raman scattering [9–11,17].

To date, most of the experimental papers on resonance Raman scattering have shown a relatively few isolated spectra above and below the excitation threshold; we present here a comprehensive data set showing the evolution of x-ray scattering to x-ray fluorescence in a free atom [18]. Results are presented for both Xe $L\alpha_{1,2}$ ($L_3M_{4,5}$) and Xe $L\beta_{2,15}$ ($L_3N_{4,5}$) x-ray emission as the excitation energy is scanned across the L_3 edge.

EXPERIMENT

The experiments described here were performed at beamline X-24A of the National Synchrotron Light Source at Brookhaven National Laboratory. The beamline consists of a double-crystal monochromator with interchangeable crystals and associated focusing optics [19–21]. For these measurements a pair of Ge(111) crystals was used, giving a resolution of about 2 eV. The output from the beamline was directed through a second carbon foil, then through a gas cell containing approximately 27 kPa xenon and finally through a second carbon foil. Photocurrents from the foils were used to measure both the incident photon flux and the Xe absorption spectrum. The gas cell was made from stainless steel with the photon beam entering and exiting the cell through thin Mylar windows. Scattered and fluorescent x rays were observed through a third Mylar window at right angles to both the direction and e vector of the linearly polarized photon beam. The emitted x rays were dispersed using a

*Permanent address: E.P.S.R.C. Daresbury Laboratory, Warrington, WA4 4AD, United Kingdom.

†Present address: Department of Physics, University of Tennessee, Knoxville, TN 37996.

‡Present address: Photon Factory, National Laboratory for High Energy Physics, Oho, Tsukuba, Ibaraki 305, Japan.

§Deceased.

Ge (220) curved-crystal monochromator [22] and detected on a position-sensitive proportional counter (PSPC) [23]. Figure 1 shows a schematic representation of the beamline and spectrometer layout.

For Xe $L\alpha_{1,2}$ spectra, the dispersion and sensitivity across the PSPC were measured by recording elastic x-ray scattering from air introduced into the gas cell. The PSPC and secondary crystal monochromator were positioned as required for recording Xe $L\alpha_{1,2}$ spectra, while a series of elastically scattered peaks were recorded between 4080 and 4140 eV. The intensity and position of each peak of the series on the PSPC were used to create energy and intensity calibration curves for the instrument. Minor corrections were made for variations of the photoemission efficiency of graphite and of the elastic-scattering cross section of N_2 [24]. The measured resolution of the elastic-scattering spectra was 2.6 eV [full width at half maximum (FWHM)], arising from a combination of primary and secondary monochromator resolutions.

Individual fluorescence spectra were recorded by setting the incoming photon energy to the desired value and recording a frame from the PSPC of the secondary monochromator. Before each such spectrum was recorded, the primary monochromator was calibrated by recording a Xe L_3 x-ray-absorption spectrum by measuring the drain currents from the two graphite films. The maximum in this absorption spectrum was used as a temporary set point. Spectra were later put on an absolute energy scale using the Xe L_3-edge absorption spectrum of Breinig *et al.* [25] who have measured the absorption maximum at 4785.2±0.6 eV, the binding energy at 4786.3±0.6 eV, and the 5*d* resonance at 4784.2±0.6 eV. In this way Xe $L\alpha_{1,2}$ spectra were recorded at excitation energies from approximately 4770 to 4830 eV. The spectra were, in general, recorded every 1.47 eV except for the five spectra around the absorption peak which were recorded at a separation of 0.73 eV. The four spectra at the highest excitation energies were recorded with a separation of approximately 5.9 eV. Each spectrum was normalized by the drain current from the incident flux monitor (carbon foil) after allowing for the varying efficiency of the monitor with photon energy. The energy window of the PSPC, when attached to the secondary monochromator in its present configuration, is about 40 eV wide. Therefore, in order to observe the evolution of the resonance Raman scattering, it was necessary to slightly adjust the angular position of the secondary monochromator when observing fluorescence excited above the L_3 edge. Several fluorescence spectra were recorded at each excitation energy throughout the experiment, and the intensities of each match to better than 10%. The data presented are the sum of all spectra recorded at each individual excitation energy.

A similar procedure was used to record the Xe $L\beta_{2,15}$ spectra, except that the region of interest was sufficiently narrow that the secondary monochromator did not have to be repositioned during the experiment. The spectra were, in general, recorded every 1.47 eV except that the four spectra at the highest excitation energies were recorded with a separation of approximately 5.9 eV. To calibrate the dispersion and relative efficiency across the PSPC, elastic scattering was measured in the region 4680–4760 eV from the 27 kPa of xenon introduced into the gas cell. Minor corrections were again made for variations in efficiency of the carbon foil and Xe elastic-scattering cross section [24]. The measured resolution of the elastically scattered spectra was about 2.6 eV (FWHM).

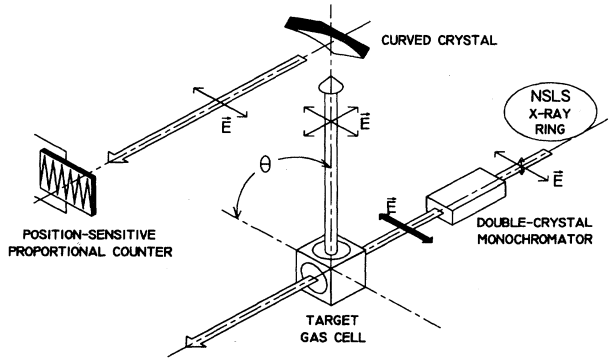

FIG. 1. Schematic layout of the X-24A beamline and experimental apparatus. X-ray emission was observed at a fixed angle of $\theta=90°$.

RESULTS

Figure 2 shows a Xe $L\alpha_{1,2}$ emission spectrum recorded ≈27 eV above the L_3 absorption edge. In the two-step model, the first step in the production of such a spectrum is excitation into the continuum of a 2*p* electron, leaving a $2p_{3/2}$ vacancy. (The *LS* coupling scheme is used for convenience and to allow comparison with previous work [4,8,9]; it is not appropriate for an atom as heavy as xenon.) A $3d_{5/2}$ or $3d_{3/2}$ electron can then drop to fill this vacancy with the accompanying emission of a photon

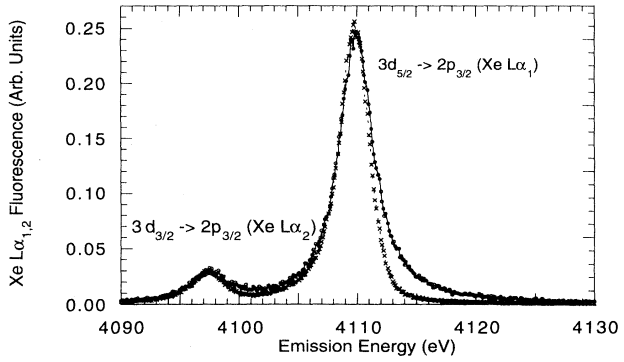

FIG. 2. Xe $L\alpha_{1,2}$ x-ray-emission spectrum (circles) recorded ≈27 eV above the L_3 edge to show the appearance of characteristic x-ray fluorescence. The data were recorded in 500 s and the peak maximum corresponds to ≈3000 counts. Also shown (crosses) is an emission spectrum recorded at 4784.5 eV, between the 5*d* resonance and the maximum at the L_3 absorption edge. The two spectra were normalized to the same peak height in this figure.

($L\alpha_{1,2}$ fluorescence). The ejected electron takes away the excess energy $h\nu - I(2p_{3/2})$, so that the $L\alpha_1$ and $L\alpha_2$ lines appear at

$$I(2p_{3/2}) - I(3d_{5/2}) = 4110.09 \pm 0.02 \text{ eV}$$

and

$$I(2p_{3/2}) - I(3d_{3/2}) = 4097.38 \pm 0.03 \text{ eV},$$

respectively, where $I(nl_j)$ is the subshell ionization energy [26]. The natural width of an x-ray line represents the sum of the widths of the initial and final states of the transition, with the width of an atomic state containing an inner-shell vacancy being determined by the lifetime of the hole through the Heisenberg uncertainty relation. Thus, in the absence of instrumental effects, the peaks in Fig. 2 will appear as symmetric, Lorentzian peaks with a half-width that reflects the lifetime of the $2p_{3/2}$ hole (2.9 eV) plus the lifetime of the resulting $3d_{5/2}$ or $3d_{3/2}$ hole state (0.5 eV) [27,28], giving an overall width of 3.4 eV.

Similarly, $L\beta_{2,15}$ fluorescence is emitted when a $4d_{5/2}$ or $4d_{3/2}$ electron fills the $2p_{3/2}$ vacancy. Figure 3 shows an $L\beta_{2,15}$ spectrum recorded ≈ 27 eV above the L_3 edge. The 0.1 eV lifetime width of the $4d_{5/2}$ or $4d_{3/2}$ final hole state combined with the 2.9 eV width of the $2p_{3/2}$ hole state results in a 3.0 eV lifetime width for these transitions [27,28]. The $L\beta_2$ and $L\beta_{15}$ components are separated by ≈ 2 eV and are not resolved. The emission energy scale for the $L\beta_{2,15}$ spectra was referenced to the value 4718.86 ± 0.08 eV for the $L\beta_2$ transition [27].

The Xe L_3 absorption edge is made up of absorption to Rydberg series converging to the continuum and from absorption to the continuum itself. Breinig *et al.* [25] have measured the Xe L_3 absorption edge and analyzed their data in terms of the first few Rydberg absorptions ($6s, 5d, 6d, 7d$) and absorption to the continuum. Their results are reproduced as Fig. 4. The short lifetime of the

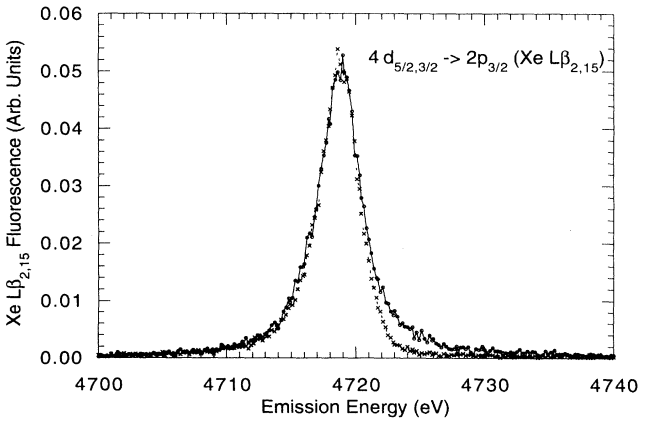

FIG. 3. Xe $L\beta_{2,15}$ x-ray-emission spectrum (circles) recorded ≈ 27 eV above the L_3 edge to show the appearance of characteristic x-ray fluorescence. The data were recorded in 500 s and the peak maximum corresponds to ≈ 800 counts. Also shown (crosses) is an emission spectrum recorded at 4785.2 eV, near the maximum at the L_3 absorption edge. The two spectra were normalized to the same peak height in this figure.

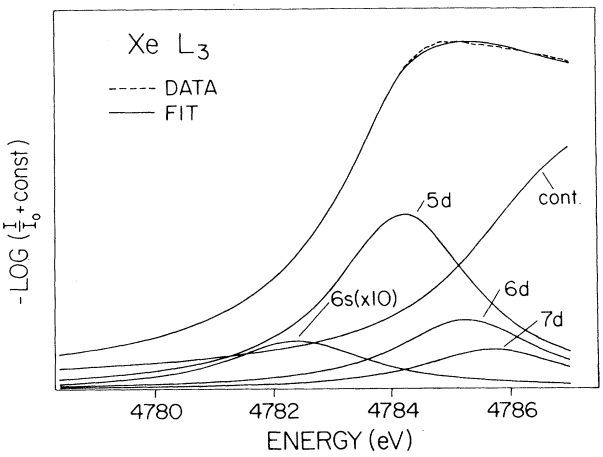

FIG. 4. Xe L_3 absorption edge and theoretical fit of component absorption profiles, taken from Breinig *et al.* [25] with permission.

$2p$ hole means that absorption of a photon near the L_3 edge (4770–4790 eV) has a finite probability of exciting any of the Rydberg levels or the continuum. We have recorded the Xe $L\alpha_{1,2}$ and $L\beta_{2,15}$ emission as the excitation energy was scanned across the L_3 absorption edge to show the evolution of the resulting emission from resonance Raman scattering (RRS), involving Rydberg excitations, through continuous resonance Raman scattering (cRRS), involving continuum excitation near threshold, to the characteristic fluorescence region.

Figures 5–8 show the results for Xe $L\alpha_{1,2}$ and $L\beta_{2,15}$ emission. Figures 5 and 7 show perspective plots of the [three-dimensional (3D)] data sets, while Figs. 6 and 8 show contour plots of the same data sets. The perspective plots are presented to allow easier comparison with the calculated resonance Raman spectra of Tulkki, Åberg, and Cowan [4,6–9]. Although the calculations those authors present are for atoms other than xenon, the resonant Raman processes are the same and the same

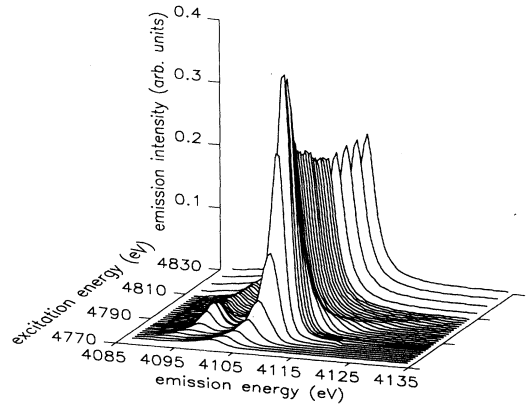

FIG. 5. A perspective plot showing the variation of Xe $L\alpha_{1,2}$ x-ray emission across the L_3 absorption edge to illustrate resonance Raman scattering and the onset of characteristic fluorescence.

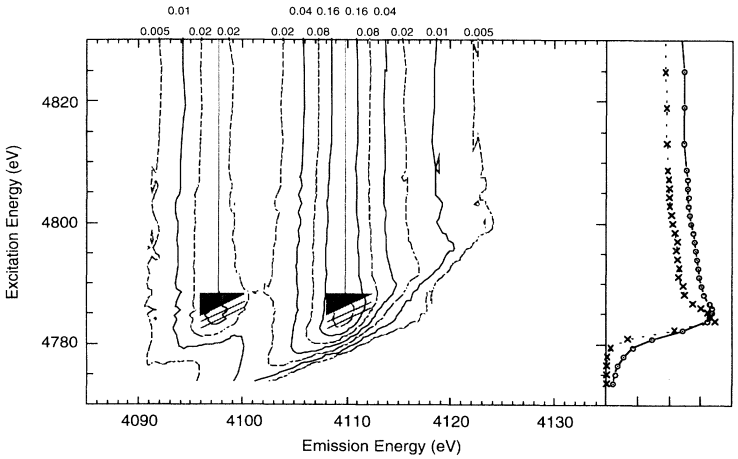

FIG. 6. A contour plot of the same data as Fig. 5, showing the variation of Xe $L\alpha_{1,2}$ x-ray emission across the L_3 absorption edge. The intensity contours are at 0.005, 0.01, 0.02, 0.04, 0.08, 0.16, and 0.32 (arbitrary units). The meanings of the superimposed lines and shaded area are explained in the text. The side panel shows the total Xe $L\alpha_{1,2}$ x-ray-emission intensity (circles) and emission intensity at 4110±0.3 eV only (crosses) as functions of excitation energy.

features are observed. On the contour plots, the gray diagonal lines show where RRS may be expected from excitation to the 5*d* and 6*d* orbitals, and the shaded triangular regions indicate the area where cRRS will be apparent (i.e., the area where the 2*p* electron is ionized but where the bandwidth of the fluorescence is energetically limited). The projections of the lengths of the diagonal lines onto the excitation-energy axis represent the full width at half maximum of the absorption to these Rydberg states [25]. The gray vertical lines show the area where characteristic fluorescence may be expected and extend from the ionization potential to higher energies. As described above and as shown in Figs. 6 and 8, these areas all overlap and thus no feature may be described as being purely due to RRS or cRRS, except that weak RRS components can be seen extending into the continuum. The total $L\alpha_{1,2}$ or $L\beta_{2,15}$ fluorescent intensity as the excitation energy is scanned gives a standard fluorescence excitation spectrum. These results are shown on the right-hand edge of the contour plots, while a plot of only the fluorescence intensity occurring at 4110±0.3 eV ($L\alpha_1$, Fig. 6) or 4719±0.3 eV ($L\beta_{2,15}$, Fig. 8) is also shown. This shows narrowing of the excitation profile as the fluorescent energy is better defined, demonstrating that excitation spectra and absorption spectra can be distinct [29].

The origins of the effects shown in Figs. 5–8 are briefly explained as follows [6–9]. If the incident energy is chosen to excite the 2*p* electron to the vacant 5*d* orbital, or any of the other vacant orbitals [25], then the situation is modified from that pertaining to x-ray fluorescence (Figs. 2 and 3). The natural width of the $2p \rightarrow 5d$ absorption resonance is, to first approximation, that of the 2*p* hole, so if one could excite the 5*d* resonance with "white" light the resulting fluorescence again would have a width characteristic of the 2*p* hole plus that of the 3*d* (or 4*d*) hole. However, if an excitation source with a narrower bandwidth than the 2*p* hole is used, the situation is different; conservation of energy then implies that the resulting fluorescence has a bandwidth equal to the uncertainty in the energy of the final atomic state convoluted with the bandwidth of the exciting radiation. In principle, RRS bandwidths as narrow as 0.5 eV (for 3*d* final states) or 0.1 eV (for 4*d* final states) would be observed if the bandwidths of the incident radiation and of the emission spectrometer were negligibly small. This effect is analogous to the case of resonance fluorescence [9–11,17]. Additionally, the fluorescence peak position must track linearly with the excitation energy as different parts of the absorption profile are investigated, which is the well-known linear dispersion of resonance fluorescence. Since the position, width, and shape of the RRS peaks depend on the energy and bandwidth of the excitation source, and the lifetime-limited width is that of the 3*d* (or 4*d*) hole rather than that of the 2*p* hole, x-ray absorption and emission in RRS are not independent processes but occur in a single quantum process [9–11,17].

The situation for continuous resonance Raman scattering is similar [6–9]. The excitation photon picks out a specific part of the continuum absorption profile, with $L\alpha_{1,2}$ or $L\beta_{2,15}$ fluorescence following. Energy conservation again limits the bandwidth of the fluorescence, but this time only on the high-energy side of a peak. On the low-energy side, fluorescence can still occur beyond the instrumental and 3*d* (or 4*d*) lifetime resolutions, with the

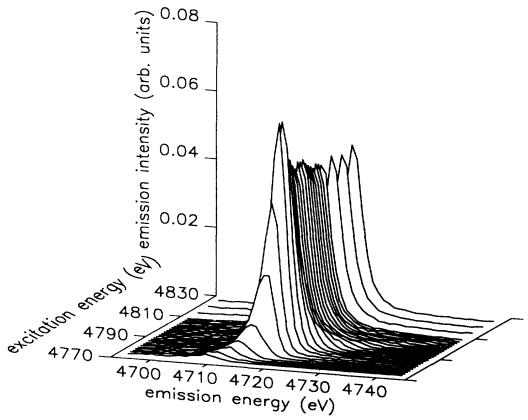

FIG. 7. A perspective plot showing the variation of Xe $L\beta_{2,15}$ x-ray emission across the L_3 absorption edge to illustrate resonance Raman scattering and the onset of characteristic fluorescence.

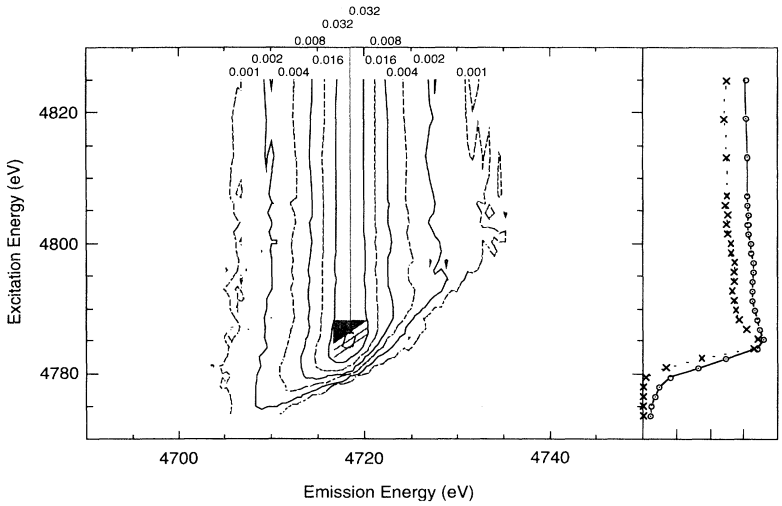

FIG. 8. A contour plot of the same data as Fig. 7, showing the variation of Xe $L\beta_{2,15}$ x-ray emission across the L_3 absorption edge. The intensity contours are at 0.001, 0.002, 0.004, 0.008, 0.016, 0.032, and 0.064 (arbitrary units). The meanings of the superimposed lines and shaded area are explained in the text. The side panel shows the total Xe $L\beta_{2,15}$ x-ray-emission intensity (circles) and emission intensity at 4719±0.3 eV only (crosses) as functions of excitation energy.

energy discrepancy being taken up by the free photoelectron. This causes the peak narrowing and asymmetric peak shapes that are associated with cRRS [6–9]. As the excitation energy is scanned across the absorption edge, more and more of the full fluorescence bandwidth becomes available until the process merges smoothly into characteristic fluorescence. Below the L_3 ionization energy, the excitation occurs in the low-energy wing of the continuum absorption, and the peak of the observed fluorescence will again track the excitation energy as different parts of the continuum absorption profile are probed. Once the ionization potential has been reached, the fluorescence peak maximum position will remain constant and only the width or tail of the fluorescence peak will increase on the high-energy side as the photoelectron carries off excess energy. Such a linear dispersion of the fluorescence peak position, followed by an unchanging peak position, is typical of cRRS [6–9]. The areas shaded gray in Figs. 6 and 8 show where fluorescence following absorption into the L_3 continuum will be modified by cRRS; again, the projections of the shaded area onto the excitation-energy and fluorescence-energy axes show the half-height points on the absorption and fluorescence profiles [25–28]. Figure 2 shows the asymmetric peak narrowing associated with cRRS; the circles show fluorescence spectra recorded following excitation well above ($\approx$27 eV) the L_3 edge, while the crosses show fluorescence following excitation at 4784.5 eV (between the 5*d* resonance and the absorption maximum). This clearly shows that for x-ray emission excited near the absorption edge, the high-energy tail of the emission is severely clipped, so not all fluorescence energies are accessible. The slight narrowing on the low-energy side of the $L\alpha_1$ peak is attributed to the contribution the 5*d* resonance makes to the overall absorption, although the clipping of the high-energy tail of the $L\alpha_2$ line must also contribute. Similar effects for $L\beta_{2,15}$ emission are shown in Fig. 3, which compares a spectrum recorded $\approx$27 eV above the L_3 edge with one recorded at the absorption maximum (4785.2 eV) near threshold.

Figure 9 shows the recorded peak position of the $L\alpha_1$ emission spectrum as a function of excitation energy and a similar plot for the $L\beta_{2,15}$ transition. This clearly shows that the $L\alpha_1$ and $L\beta_{2,15}$ peaks exhibit Raman-scattering-type linear dispersion below threshold before they level off into fluorescent behavior. However, it must be noted that the slope of the observed dispersion is not unity, but is rather 1.16 for the $L\alpha_1$ peak and 1.17 for the $L\beta_{2,15}$ peak. This is attributed to the overlap of the accessible spectral features; as the excitation energy is increased, the dominant absorption changes from excita-

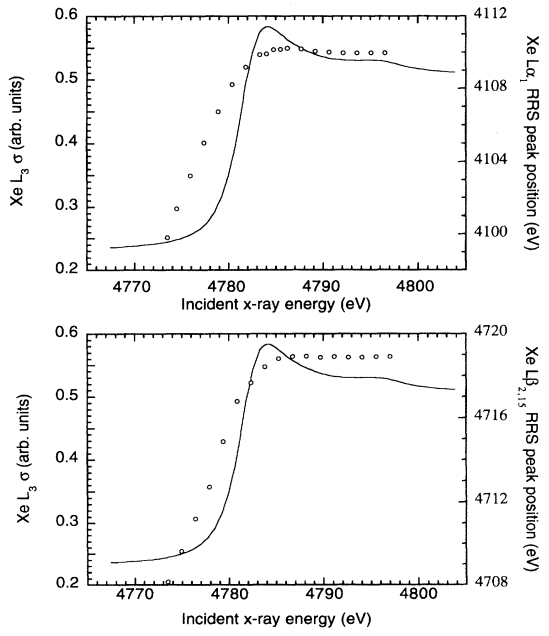

FIG. 9. Upper part: Variation of the position of the peak of the Xe $L\alpha_1$ x-ray-emission spectrum as the incident x-ray energy is scanned across the L_3 edge (circles, right-hand scale) superimposed on the Xe L_3 absorption spectrum (line, left-hand scale) for comparison. Lower part: Same as upper frame except that the position of the Xe $L\beta_{2,15}$ peak is plotted (circles, right-hand scale).

tion of the 5*d* orbital, through the 6*d* and 7*d* orbitals, until finally absorption into the continuum is dominant. Thus we observe the emission mechanism evolve from RRS through cRRS to characteristic fluorescence.

The sharpening of the excitation profiles for selected narrow fluorescence bands, show in Figs. 6 and 8, is an effect similar to the results described by Hämäläinen *et al.* [29]. We note that such measurements may be affected by shifting fluorescence peak profiles due to RRS and cRRS below threshold. However, by recording the entire fluorescence spectrum as a function of excitation energy, it is possible to determine the excitation spectrum for any selected range of fluorescence energies. In this technique, however, consideration must be given to the smearing effects on the excitation profiles of the finite resolutions of the incident radiation and of the emission spectrometer.

In summary, we have recorded complete sets of x-ray emission spectra across the Xe L_3 edge which display resonance and threshold features and the onset of characteristic fluorescence. The theory for these processes has been presented by Tulkki and Åberg in terms of full transition matrix elements and generalized Kramers-Heisenberg scattering cross sections [6–9]. The results presented here are consistent with these theoretical descriptions.

ACKNOWLEDGMENTS

These measurements were made at the National Synchrotron Light Source at Brookhaven National Laboratory, which is supported by the U.S. Department of Energy, Division of Materials Sciences and Division of Chemical Sciences. This work was supported in part by the U.S. Department of Energy, Office of Basic Sciences under Contract No. W-31-109-Eng-38. Thanks must be expressed to Professor B. Crasemann for permission to reproduce Fig. 4 and for supplying copies of the original figure. Professor T. Åberg and Professor B. Crasemann also deserve thanks for helpful discussions and supplying copies of their paper in press. M.McD. would like to thank Daresbury Laboratory for permission to take extended leave to perform this work.

[1] C. J. Sparks, Jr., Phys. Rev. Lett. **33**, 262 (1974).
[2] P. Eisenberger, P. M. Platzman, and H. Winick, Phys. Rev. Lett. **36**, 623 (1976).
[3] H. Czerwinski, F. Smend, D. Schaupp, M. Schumacher, A. H. Millhouse, and H. Schenk-Strauss, Z. Phys. A **322**, 183 (1985).
[4] P. L. Cowan, in *Resonant Anomalous X-Ray Scattering: Theory and Applications,* edited by G. Materlik, C. J. Sparks, and K. Fischer (North-Holland, Amsterdam, 1994), p. 449.
[5] T. Åberg, Phys. Scr. **21**, 495 (1980).
[6] J. Tulkki and T. Åberg, J. Phys. B **15**, L435 (1982).
[7] J. Tulkki, Phys. Rev. A **27**, 3375 (1983).
[8] T. Åberg and J. Tulkki, in *Atomic Inner-Shell Physics,* edited by B. Crasemann (Plenum, New York, 1985), pp. 419–463.
[9] T. Åberg and B. Crasemann, in *Resonant Anomalous X-Ray Scattering: Theory and Applications* [4], p. 431.
[10] G. S. Brown, M. H. Chen, B. Crasemann, and G. E. Ice, Phys. Rev. Lett. **45**, 1937 (1980).
[11] G. B. Armen, T. Åberg, J. C. Levin, B. Crasemann, M. H. Chen, G. E. Ice, and G. S. Brown, Phys. Rev. Lett. **54**, 1142 (1985).
[12] D. Cubric, A. A. Wills, E. Sokell, J. Comer, and M. A. MacDonald, J. Phys. B **26**, 4425 (1993).
[13] A. Kivimäki, A. Naves de Brito, S. Aksela, H. Aksela, O.-P. Sairanen, A. Ausmees, S. J. Osborne, L. B. Dantas, and S. Svensson, Phys. Rev. Lett. **71**, 4307 (1993).
[14] Z. F. Liu, G. M. Bancroft, K. H. Tan, and M. Schachter, Phys. Rev. Lett. **72**, 621 (1994).
[15] T. LeBrun, S. H. Southworth, M. A. MacDonald, and Y. Azuma (unpublished).
[16] T. Åberg, Phys. Scr. **T41**, 71 (1992).
[17] W. Heitler, *The Quantum Theory of Radiation* (Clarendon, Oxford, 1954).
[18] A brief report on some of these data was given by S. H. Southworth, Nucl. Instrum. Methods Phys. Res. Sect. B **87**, 247 (1994).
[19] P. L. Cowan, J. B. Hastings, T. Jach, and J. P. Kirkland, Nucl. Instrum. Methods Phys. Res. **208**, 349 (1983).
[20] P. L. Cowan, S. Brennan, R. D. Deslattes, A. Henins, T. Jach, and E. G. Kessler, Nucl. Instrum. Methods Phys. Res. Sect. A **246**, 154 (1986).
[21] P. L. Cowan, S. Brennan, T. Jach, D. W. Lindle, and B. A. Karlin, Rev. Sci. Instrum. **60**, 1603 (1989).
[22] S. Brennan, P. L. Cowan, R. D. Deslattes, A. Henins, D. W. Lindle, and B. A. Karlin, Rev. Sci. Instrum. **60**, 2243 (1989).
[23] B. P. Duval, J. Barth, R. D. Deslattes, A. Henins, and G. G. Luther, Nucl. Instrum. Methods Phys. Res. **222**, 274 (1984).
[24] J. H. Hubbell, W. J. Veigele, E. A. Briggs, R. T. Brown, D. T. Cromer, and R. J. Howerton, J. Phys. Chem. Ref. Data **4**, 471 (1975).
[25] M. Breinig, M. H. Chen, G. E. Ice, F. Parente, B. Crasemann, and G. S. Brown, Phys. Rev. A **22**, 520 (1980).
[26] T. Mooney, E. Lindroth, P. Indelicato, E. G. Kessler, Jr., and R. D. Deslattes, Phys. Rev. A **45**, 1531 (1992).
[27] M. Ohno and R. E. LaVilla, Phys. Rev. A **45**, 4713 (1992).
[28] K. Siegbahn, C. Nordling, G. Johansson, J. Hedman, P. R. Heden, K. Hamrin, U. Gelius, T. Bergmark, L. O. Werme, R. Manne, and Y. Baer, *ESCA Applied to Free Molecules* (North-Holland, Amsterdam, 1969).
[29] K. Hämäläinen, D. P. Siddons, J. B. Hastings, and L. E. Berman, Phys. Rev. Lett. **67**, 2850 (1991).